Spectral Prediction and Notching of RF Emitters for Cognitive Radar Coexistence

Jacob A. Kovarskiy[1], Jonathan W. Owen[2], Ram M. Narayanan[1], Shannon D. Blunt[2], Anthony F. Martone[3], Kelly D. Sherbondy[3]
[1]Dept. of Electrical Engineering, The Pennsylvania State University, University Park, PA, USA
[2] Radar Systems Lab (RSL), University of Kansas, Lawrence, KS, USA
[3] Army Research Laboratory, Sensors and Electronic Devices Directorate, Adelphi, MD, USA

***Abstract*—The increasing demand for radio frequency (RF) spectrum requires radars to coexist with interfering RF emitters. Innovations in waveform design paired with dynamic spectrum access techniques allow for efficient spectrum sharing for radar. This work evaluates a recently developed real-time implementation of spectrum sharing cognitive radar using commercial-of-the-shelf (COTS) hardware. Prediction of coexisting RF emitter frequencies informs the design of spectrally notched FM noise waveforms on transmit. Waveform notches are optimized on a pulse-to-pulse basis while accounting for the zero-order hold model inherent to lower fidelity digital-to-analog converters to ensure desired reconstruction. The radar system employs cognition to learn and predict RF emitter activity via a stochastic model-based approach. Initially, passive spectrum observations are used to estimate a stochastic model which is then exploited to predict the likelihood of future RF activity. The benefits and limitations of this sense-predict-and-notch (SPAN) approach are evaluated using a set of synthetic interference scenarios in real-time.**

***Index Terms*—cognitive radar, spectrum sharing, spectrum prediction, noise radar, spectral notching**

I. Introduction

Recent developments in wireless technologies have rapidly increased demand for the radio frequency (RF) spectrum as a resource [1]. As more devices become integrated with wireless capabilities, improvements in existing technology (such as 5G networks) require higher data throughput and therefore bandwidth. In response, new Federal Communications Commission (FCC) policies allow commercial communication networks to share spectrum with incumbent radar systems at the 3.5 GHz and 5 GHz bands [2], [3]. However, coexisting radar and communication emitters could mutually interfere with one another, thus causing degradation of target detection for the radar [4], [5]. Spectrum sharing is executed via dynamic spectrum access (DSA), which exploits available spectrum during periods of inactivity [6]. Efficient and robust DSA implementations apply cognition to the coexistence problem, where cognition is characterized by a perception-action cycle (PAC) that iteratively senses, learns, and adapts to a changing environment [7]. This work considers a cognitive radar employing the PAC in a dynamic RF environment to avoid interference.

Cognitive radar for DSA requires a pair of spectrum processing and waveform decision techniques to operate within a congested environment. Spectrum processing refers to techniques for accurately sensing and monitoring RF interference (RFI). Here we utilize a stochastic model-based approach to sense and predict the likelihood of future interference. The model represents the RF spectrum as a set of alternating renewal processes that switch between two states: busy and idle. RFI is initially detected and monitored over time to measure model parameters. This predictive model identifies unused frequency subbands with potential for utilization by the radar. Given these predicted subbands, the waveform decision technique determines the optimal transmit waveform based on a signal-to-interference plus noise ratio (SINR) and bandwidth trade-off.

Previous work has demonstrated that a reactive avoidance technique that transmits a linear frequency modulated (LFM) chirp at the widest contiguous cluster of available RF bandwidth can effectively reduce mutual interference between the cognitive radar and other RF emitters in real-time using commercial-of-the-shelf (COTS) hardware [8], [5], [9]. The RFI avoidance framework using LFM waveforms has also been combined with stochastic model-based prediction to operate with enhanced real-time performance [10], [11]. Reactive spectrum processing poses an alternative to prediction by identifying available bandwidth based only upon detected changes in the environment. While reaction requires fewer computational resources, prediction may mitigate erroneous waveform decisions during RF state transitions and reduce response latency.

The performance benefits of employing notched random FM waveforms with a reactive spectrum processing framework have likewise been recently demonstrated [12], [13]. Here, the cognitive radar utilizes notched frequency modulated (FM) noise waveforms on transmit to mitigate mutual interference. These waveforms use the maximum bandwidth of interest while placing spectral notches that coincide with RFI. Specifically, pseudo-random optimized (PRO) FM waveforms [14] are generated and sequentially notched using zero-order reconstruction of waveforms (ZOROW) [15], which leverages the efficient notching scheme of [16] while accounting for the impact of lower fidelity hardware. As a result, the system can achieve finer range resolution during radar processing.

This work employs stochastic model-based prediction in conjunction with the notched random FM waveform transmit framework in a real-time COTS hardware implementation. Spectrum prediction seeks to mitigate performance degradation caused by additional latency associated with the notching approach. Similarly, notching allows the system to occupy greater bandwidth relative to the sense-predict-and-avoid (SPAA) approach in [10]. The sense-predict-and-notch (SPAN) cognitive radar strategy is evaluated using real-time experiments with synthetic RFI scenarios.

II. Spectrum Prediction Model

To perform spectrum sharing, this cognitive radar initially senses and monitors RF activity over multiple frequency channels. These observations are used to estimate a stochastic model describing the spectrum over time. Once the model is learned, the system proceeds with the PAC by iteratively sensing RFI, predicting available bandwidth, and accessing the spectrum. This process requires continuous spectrum measurements consisting of N-point frequency domain observations denoted by $Y[n]$. The spectrum is partitioned into M channels to monitor RF activity in each individual subband. Each channel's start and end index is defined by $N_\mathrm{s} = \{N_{\mathrm{s}_1}, N_{\mathrm{s}_2}, ..., N_{\mathrm{s}_M}\}$ and $N_\mathrm{e} = \{N_{\mathrm{e}_1}, N_{\mathrm{e}_2}, ..., N_{\mathrm{e}_M}\}$, respectively. To sense the presence of RFI, the system applies energy detection to each channel [17]. Each RF channel state is represented as a set of M binary states $S = \{S_1, S_2, ..., S_M\}$ for every spectrum measurement. Energy detection estimates the energy in each channel by applying a detection threshold λ_D to determine the respective states:

$$S_i = \left(\sum_{n=N_{\mathrm{s}_i}}^{N_{\mathrm{e}_i}} |Y[n]|^2 \right) \underset{\text{OFF}}{\overset{\text{ON}}{\gtrless}} \lambda_D \quad \forall i \in \{1, 2, ..., M\}. \tag{1}$$

A channel in the ON state is busy and unavailable for radar access, while an OFF state denotes an idle channel that is available for access. The system retains memory of the set of continuously detected channel states S over time. This time-varying history of channel states allows the system to model RF activity.

This work generalizes the arrival and departure of RFI as a set of alternating renewal processes. Each channel alternates between busy and idle with independently random time intervals between state transitions. A pair of sets $B = \{B_{\mathrm{t}1}, B_{\mathrm{t}2}, ...B_{\mathrm{t}M}\}$ and $I = \{I_{\mathrm{t}1}, I_{\mathrm{t}2}, ...I_{\mathrm{t}M}\}$ contain independent random variables that describe the *busy* and *idle* time distributions in each channel. With a parametric modeling approach, each channel's distribution pair $B_{\mathrm{t}i} \sim N(\mu_{\mathrm{B}i}, \sigma^2_{\mathrm{B}i})$ and $I_{\mathrm{t}i} \sim N(\mu_{\mathrm{I}i}, \sigma^2_{\mathrm{I}i})$ is assumed to be normally distributed. The system uses the collection of RF channel states S over time to count the duration of each respective busy and idle interval. Sample mean estimates $\mu_{\mathrm{B}i}, \mu_{\mathrm{I}i}$ and variance estimates $\sigma^2_{\mathrm{B}i}, \sigma^2_{\mathrm{I}i}$ are obtained for each i^{th} channel using these measured busy and idle intervals (Fig. 1). After estimating these parameters, the system generates a pair of Gaussian cumulative distribution

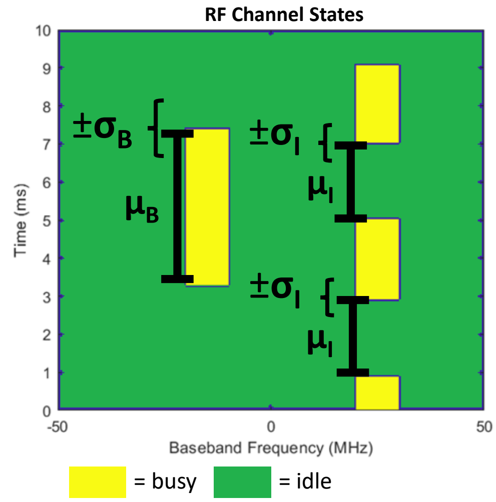

Fig. 1. Visual example of two switching RF emitters after detection over time. μ_B and σ_B describe busy interval statistics μ_I and σ_I describe idle statistics. Each contiguous busy and idle block describes individual B_t and I_t observations, respectively.

functions (CDFs) to describe the probability of the i^{th} channel remaining in a busy or idle state for $t_{\mathrm{B}i}$ or $t_{\mathrm{I}i}$:

$$\begin{aligned} p_{\mathrm{B}i}(t_{\mathrm{B}i}) &= \frac{1}{\sigma_{\mathrm{B}i}\sqrt{2\pi}} \int_{-\infty}^{t_{\mathrm{B}i}} \exp\left(-\frac{t-\mu_{\mathrm{B}i}}{2\sigma^2_{\mathrm{B}i}}\right) dt \\ p_{\mathrm{I}i}(t_{\mathrm{I}i}) &= \frac{1}{\sigma_{\mathrm{I}i}\sqrt{2\pi}} \int_{-\infty}^{t_{\mathrm{I}i}} \exp\left(-\frac{t-\mu_{\mathrm{I}i}}{2\sigma^2_{\mathrm{I}i}}\right) dt. \end{aligned} \tag{2}$$

Initially, the system estimates the mean and variance parameters for (2) during a passive observation period where no radar transmission occurs. After this phase, the radar periodically transmits pulses with notches according to the stochastic model. From here, the system continues to monitor the RF states S and track the duration of each channel's respective state. Prior to transmitting a radar pulse, the likelihood of each i^{th} channel's availability $p_{\mathrm{a}i}$ is computed as:

$$p_{\mathrm{a}i} = \begin{cases} p_{\mathrm{I}i}(t_{\mathrm{I}i} + t_0), & S_i = 0 \\ 1 - p_{\mathrm{B}i}(t_{\mathrm{B}i} + t_0), & S_i = 1, \end{cases} \tag{3}$$

where $t_{\mathrm{B}i}$ and $t_{\mathrm{I}i}$ describe the current time spent in a busy or idle state for each channel respectively, while t_0 describes the time until the next radar pulse. The minimum realizable t_0 is limited by the adaptation latency of the notched waveform generation method. The system then uses the set of availability likelihoods $p_{\mathrm{a}i}$ to predict a set of future channel states $A = \{A_1, A_2, ...A_M\}$:

$$A_i = \begin{cases} p_{\mathrm{a}i} \geq \theta_\mathrm{I}, & S_i = 0 \\ p_{\mathrm{a}i} \geq \theta_\mathrm{B}, & S_i = 1. \end{cases} \tag{4}$$

Using the current observed states S, each i^{th} likelihood is thresholded by θ_I and θ_B to infer the future states. These thresholds are determined via a grid search to optimize the trade-off betweens collisions and missed opportunites [10].

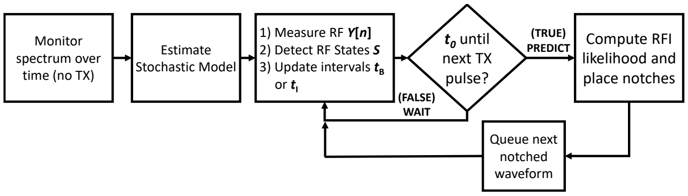

Fig. 2. Stochastic model estimation process followed by radar operation. The initial RF monitoring stage estimates the model (first two blocks), then the system begins radar operation with prediction and waveform adaptation between each pulse.

The radar places notches at channels predicted to be in a busy state or $A_i = 0$. The system periodically predicts A and begins waveform generation at t_0 before the end of each pulse repetition interval (PRI). Figure 2 describes this process of estimating the prediction model and subsequently applying prediction to radar operation.

III. Notched Waveform Design

The sense-react-and-notch (SRAN) strategy outlined in [12] leverages recent work on spectrally-shaped, random FM waveforms to place in-band spectral notches on a per-waveform basis in response to dynamic RFI. To implement the SRAN framework on an SDR platform, two random FM waveform generation methods are applied sequentially. First, the PRO-FM approach of [14], [12] is employed to produce a transmitter-suitable waveform that possesses a desirable overall power spectrum shape containing spectral notches based on an RFI identification algorithm [9]. The PRO-FM approach produces waveforms with constant modulus and adheres to a desired power spectrum template $|G(f)|^2$. While in general the template is arbitrary, this works selects a Gaussian spectral shape for $|G(f)|^2$ with notches defined by:

$$|G(f)| = \begin{cases} h_{\mathrm{L}}(f), & f \in \mathbf{\Omega}_{\mathrm{L}} \\ 0, & f \in \mathbf{\Omega} \\ h_{\mathrm{U}}(f), & f \in \mathbf{\Omega}_{\mathrm{H}}. \end{cases} \tag{5}$$

The notch location is defined by $\mathbf{\Omega}_{\mathrm{L}} < \mathbf{\Omega} < \mathbf{\Omega}_{\mathrm{U}}$, where $h_{\mathrm{L}}(f)$ and $h_{\mathrm{U}}(f)$ define lower and upper notch tapers. The constant modulus and spectral shape requirements are enforced via an alternating projection optimization technique.

To rapidly deepen the waveform spectral notches for real-time implementation on COTS hardware, the ZOROW method [15] is also utilized (Fig. 3). ZOROW accounts for the lower fidelity waveform reconstruction implied when using modest digital-to-analog converters (DACs) available in SDRs. This approach uses a signal representation that conforms to the zero-order hold model employed by the SDR DAC, in which the DAC input sample is held constant for T_{s} seconds. Taking these synthesis imperfections into consideration is important when precise notches must be reconstructed on transmit.

The waveform shaping algorithms are implemented on the field-programmable gate array (FPGA) of the SDR such that resources are efficiently utilized, desired operational timing constraints are met, and necessary notch depths imposed in

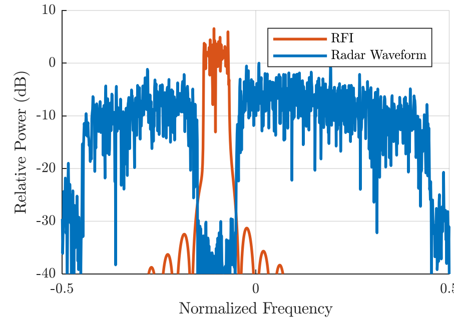

Fig. 3. Example of a sense-react-and-notch (SRAN) radar waveform generated with notches to coincide with sensed RFI.

the waveform are maximized. This waveform implementation is explained in detail in [13]. All processing was simplified to the application of fast Fourier Transforms (FFTs), inverse FFTs, multiplies, and additions in a burst streaming format. To meet the minimum timing constraints, 2 PRO-FM iterations and 6 ZOROW iterations were deemed sufficient to impose a desired spectral shape with a $\sim$25 dB notch depth relative to peak power after accounting for worst-case spectral variation. The SDR with this added waveform diversity supports pulse repetition frequencies up to 2.2 kHz, a minimum adaptation interval of 942 μs, and may incorporate multiple spectral notches per waveform.

IV. Implementation, Evaluation, and Results

A. Real-time Implementation

The SPAN cognitive radar is implemented on a USRP X310 SDR interfaced with a host PC controller. The system receives in-phase and quadrature samples at 100 MSamples/s before performing digital down-conversion to baseband. An FPGA performs a 4096-point FFT on each sequential block of data, which is then streamed to the host to allow the system to continuously monitor a 100-MHz portion of the RF spectrum. The host performs energy detection [9] and predictive processing by partitioning the spectrum into $M = 20$ separate 5 MHz wide frequency subbands. After using the model from section II to predict spectral notch locations, the respective parameters are sent to the FPGA to perform waveform optimization and generation. This FPGA implementation of notched waveform generation minimizes the computational latency of a complex process. Given a single spectrum sensing FFT duration of $T_0 = 40.96$ μs, the time to predict ahead t_0 is discretized by N_0 timesteps where $t_0 = N_0 T_0 = 491.5$ μs. Due to waveform adaptation delay, the system operates with a minimum $N_0 = 12$ timesteps and a radar PRI determined by $(N_0 - 1)T_0 = 450.6$ μs. Consequently, the radar predicts and adapts the transmit waveform every PRI.

B. System Evaluation

To test and evaluate this cognitive radar strategy, a vector signal transceiver (VST) acts as an RF environment emulator that transmits RFI. The SDR's radar transmission and VST-generated RFI feed into an RF combiner, with the resulting

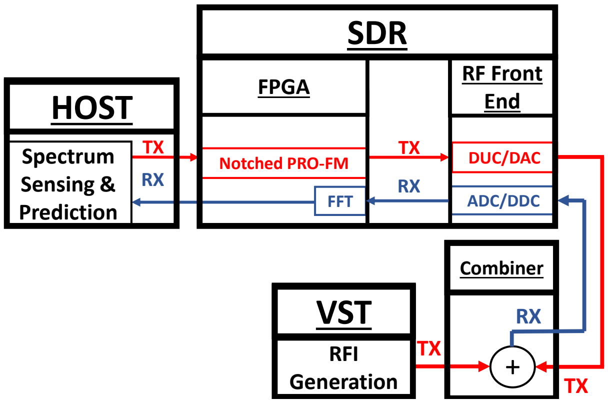

Fig. 4. Block diagram of the real-time hardware setup during testing. The receive and transmit paths as well as the processing within each hardware component is described.

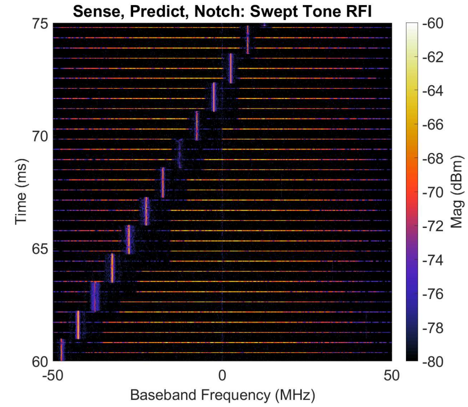

Fig. 6. Spectrogram of cognitive radar operation using a SPAN strategy on swept tone interference (819.2 µs dwell time).

signal then captured by the cognitive radar receiver (Fig. 4). This configuration allows the system to perform spectrum sharing as well as radar data capture. For these tests, the cognitive radar estimates model distributions for 410 milliseconds of RF data and performs radar operation in the subsequent 410 milliseconds.

The system is evaluated using three RFI scenarios: 1) swept tone, 2) random single tone, and 3) random two-tone. For swept tone signals, the VST continuously sweeps a sinusoid over all 20 channels with a fixed dwell time. This case demonstrates the radar's ability to predict and coexist with deterministic RFI. These performance results are discussed in Section IV-C.

The random single tone case involves a single sinusoid at -17.5 MHz baseband with a fixed on-time and randomly varying off-times, or idle intervals. Baseband refers to the waveform frequencies after the SDR performs digital down-conversion with some arbitrary carrier frequency. The idle intervals are randomly generated according to a selected mean μ_{I} and standard deviation σ_{I}. This scenario evaluates performance at increasing levels of variation characterized by the idle coefficient of variation (CoV) $c_{\mathrm{v}} = \sigma_{\mathrm{I}}/\mu_{\mathrm{I}}$. For each

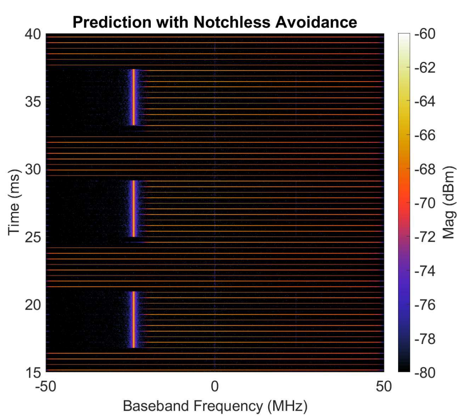

Fig. 5. Spectrogram from cognitive radar operation using a SPAA strategy. This approach leaves portions of the RF spectrum unoccupied.

fixed on-time μ_{B}, the mean idle interval is set to be equal as $\mu_{\mathrm{I}} = \mu_{\mathrm{B}}$. These performance results are discussed in Section IV-D.

Finally, for the two-tone case, the VST transmits two random switching sinusoids at -27.5 MHz and 22.5 MHz baseband. Similar to the single tone case, the on-time μ_{B} is fixed, with the randomly generated idle intervals defined by $\mu_{\mathrm{I}} = \mu_{\mathrm{B}}$ and some selected CoV $c_{\mathrm{v}} = \sigma_{\mathrm{I}}/\mu_{\mathrm{I}}$. Each tone is given independent μ_{I} and σ_{I} parameters with several tested combinations. These performance results are discussed in Section IV-E.

We consider performance metrics of collision rate, missed opportunity rate, and bandwidth improvement. A collision involves a radar waveform colliding or interfering with co-existing emitters while a missed opportunity refers to an unused open frequency channel during radar operation [8]. For this system, collisions are equivalent to a predicted missed detection or type II error and missed opportunities refer to predicted type I errors that result in falsely placed notches. The collision and missed opportunity rates validate the performance of prediction for spectrum processing.

Bandwidth improvement specifies the additional bandwidth gained by transmitting a notched waveform as opposed to notchless LFM chirp-based avoidance that selects the widest available contiguous bandwidth. For example, Fig. 5 shows unused subbands where notching using the SPAN approach should provide results with bandwidth improvement. The subsequent sections show results for the aforementioned test RFI scenarios.

C. Swept Tone RFI Results

For the swept tone RFI pattern, we evaluate dwell times of 819.2 µs, 2.05 ms, and 4.1 ms. The dwell time refers to the time spent by the RFI in each 5 MHz subband. Figure 6 demonstrates the system accurately avoiding a swept tone pattern. During RFI channel hops, the prediction approach may widen the notch to cover adjacent channels and minimize collisions. This redundant notching results in a higher missed opportunity rate compared to collisions shown in Fig. 7.

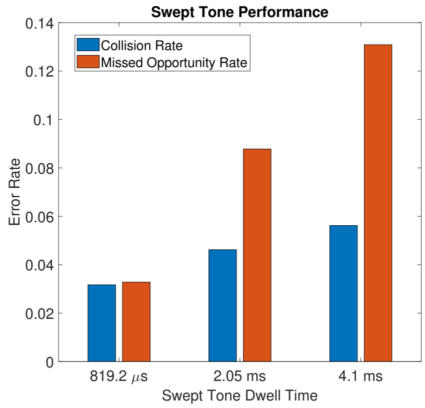

Fig. 7. Collision and missed opportunity rates for a swept tone RFI pattern with varying dwell times.

TABLE I
SWEPT TONE BANDWIDTH IMPROVEMENT OVER NOTCHLESS AVOIDANCE.

Dwell Time	819.2 µs	2.05 ms	4.1 ms
Bandwidth Improvement	20.3 MHz	19.2 MHz	17.2 MHz

The missed opportunity rate increases for longer dwell times since the system gradually widens notches in anticipation of transitions. Table I shows a significant bandwidth improvement as a result of notching compared to traditional avoidance.

D. Random Single Tone RFI Results

The random single tone RFI scenario evaluates performance with respect to the CoV c_v of the idle time interval (summarized in Fig. 9). These tests evaluated 3 sets with on-times μ_B of 819.2 µs, 2.05 ms, and 4.1 ms for a tone at -17.5 MHz. For each μ_B, the idle c_v value ranges from 0 to 1. Maintaining a fixed on-time (σ_B=0), emulates a communication system with a fixed size data burst and random time between requests for data transmission. Similar to results in [10], the missed opportunity rate increases with idle interval variation (Fig. 9(b)). The use of prediction threshold optimization results in the number of observed waveform adaptations decreasing to almost 0 (Fig. 9(d)) with a high c_v. The threshold optimization results in a reduced adaptation rate to preserve performance in highly variable scenarios. As a result, threshold selection causes the collisions (Fig. 9(a)) to decrease as variability increases. When no waveform adaptation occurs, the system places a constant notch at the RFI location. Before the system stops adapting the transmit waveform, the collision rate shows a slight increase with c_v (Fig. 9(a)). Figure 9(c) shows a significant bandwidth improvement over the notchless avoidance implementation.

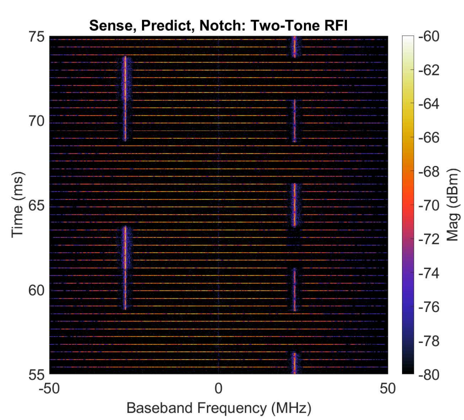

Fig. 8. Spectrogram of cognitive radar operation using a SPAN strategy on two-tone RFI.

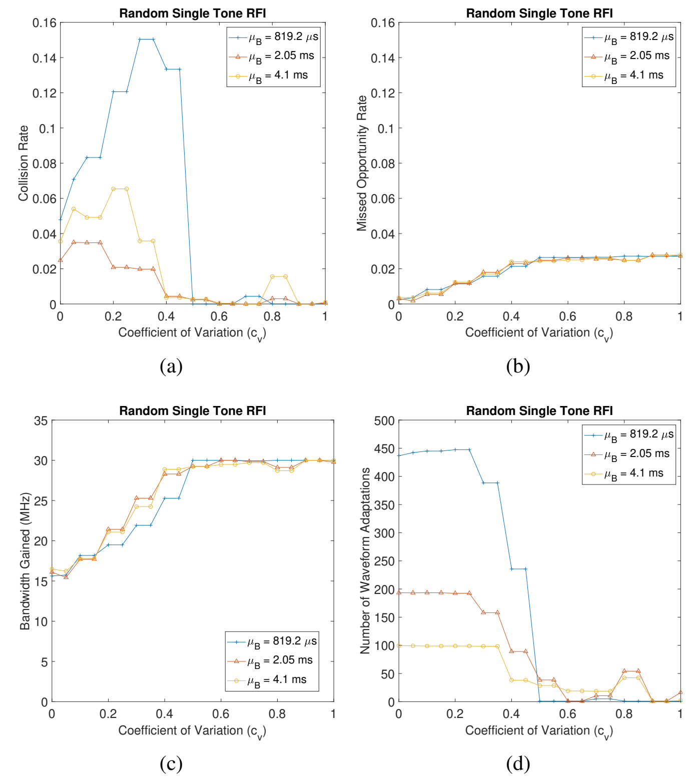

Fig. 9. Performance for the random single tone RFI in terms of (a) collision rate, (b) missed opportunity rate, (c) bandwith gained, and (d) number of waveform adaptations between pulses.

E. Random Two-tone RFI Results

Finally, the two-tone RFI scenarios evaluate performance for two sinusoids with 5 different combinations of idle time

TABLE II
TWO-TONE CASE DEFINITION AND BANDWIDTH IMPROVEMENT OVER NOTCHLESS AVOIDANCE.

	Case 1	**Case 2**	**Case 3**	**Case 4**	**Case 5**
-27.5 MHz CoV c_v	0	0	0	0.225	0.45
22.5 MHz CoV c_v	0	0.32	0.45	0.45	0.225
Bandwidth Improved (MHz)	22.8	23.2	23.4	23.8	24.0

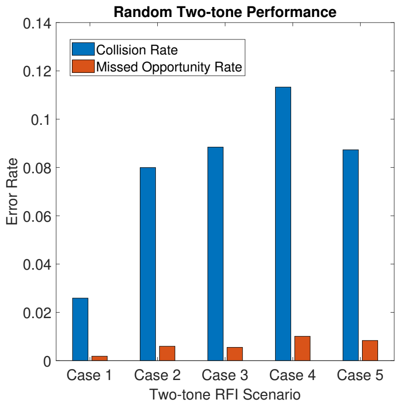

Fig. 10. Collision and missed opportunity rates for two-tone RFI with varying statistics in each case. Case statistics are shown in table II

statistics (Table II). Similar to the single tone tests, the on-time is deterministic and equal to the mean idle interval such that $\mu_{\mathrm{B}} = \mu_{\mathrm{I}}$ and $\sigma_{\mathrm{B}} = 0$. Figure 8 shows an example of this switching two-tone RFI scenario. Similar to the single tone results, performance degrades for cases with higher c_v values (Fig. 10). Per Table II, case 1 is deterministic in that $c_{\mathrm{v}} = 0$ for both tones. This case shows significantly lower missed opportunity rates than the other random cases where $c_{\mathrm{v}} > 0$. Case 4 has the highest error rates where c_{v} is largest for the shorter duration signal ($\mu_{\mathrm{B}} = 2.05$ ms). Variability for shorter duration RFI has a larger impact on cognitive radar performance than slower changing RFI. The collision rate shows slight degradation for cases with a larger c_{v}. Notching demonstrates consistent bandwidth improvement for the two-tone scenarios (Table II).

V. Conclusions

The viability and benefits of a sense-predict-and-notch (SPAN) cognitive radar strategy has been demonstrated with real-time hardware experiments. Compared to the sense-predict-and-avoid (SPAA) notchless framework, this implementation occupies higher bandwidth which results in finer range resolution during spectrum sharing. Despite additional processing latency for notching compared to LFM chirp avoidance, the system maintains prediction performance for different levels of time variation. Prediction error rates for predictive notching are comparable to the notchless avoidance results [10] despite operating with a longer PRI and double the adaptation latency. This framework allows for more efficient bandwidth utilization and mitigation of errors caused by RF state transitions. Future work will investigate employing metacognition to select a spectrum processing and waveform decision pair for spectrum sharing [18]. Some RF environments may require a system to adapt between prediction and reaction, or notching and avoidance. Additionally, performance may improve by reducing processing latency for predicting RFI and generating notched waveforms.

Acknowledgment

This work was supported by Army Research Office (ARO) grants W911NF-15-2-0066 and W911NF-15-2-0063.

References

[1] M. E. Davis, "Frequency allocation challenges for ultra-wideband radars," *IEEE Aerospace and Electronic Systems Magazine*, vol. 28, no. 7, pp. 12–18, July 2013.

[2] J. H. Reed, A. W. Clegg, A. V. Padaki, T. Yang, R. Nealy, C. Dietrich, C. R. Anderson, D. M. Mearns, "On the co-existence of TD-LTE and radar over 3.5 GHz band: an experimental study," *IEEE Wireless Communications Letters*, vol. 5, no. 4, pp. 368–371, Aug. 2016.

[3] M. Labib, J. H. Reed, A. F. Martone, A. I. Zaghloul, "Coexistence between radar and LTE-U systems: survey on the 5 GHz band," *URSI National Radio Science Meeting*, Boulder, CO, Jan. 2016.

[4] H. Wang, J. T. Johnson, C. J. Baker, "Spectrum sharing between communications and ATC radar systems," *IET Radar, Sonar, & Navigation*, vol. 11, no. 6, pp. 994–1001, July 2017.

[5] B. H. Kirk, M. A. Kozy, K. A. Gallagher, R. M. Narayanan, R. M. Buehrer, A. F. Martone, K. D. Sherbondy, "Cognitive software-defined radar: evaluation of target detection with RFI avoidance," *IEEE Radar Conf.*, Boston, MA, Apr. 2019.

[6] R. Tandra, S. M. Mishra, A. Sahai, "What is a spectrum hole and what does it take to recognize one?" *Proc. IEEE*, vol. 97, no. 5, pp. 824–848, May 2009.

[7] S. Haykin J. M. Fuster, "On cognitive dynamic systems: cognitive neuroscience and engineering learning from each other," *Proc. IEEE*, vol. 102, no. 4, pp. 608–628, April 2014.

[8] B. H. Kirk, R. M. Narayanan, K. A. Gallagher, A. F. Martone, K. D. Sherbondy, "Avoidance of time-varying radio frequency interference with software-defined cognitive radar," *IEEE Trans. Aerospace & Electronic Systems*, vol. 55, no. 3, pp. 1090–1107, June 2019.

[9] A. F. Martone, K. I. Ranney, K. D. Sherbondy, K. A. Gallagher, S. D. Blunt, "Spectrum allocation for non-cooperative radar coexistence," *IEEE Trans. Aerospace & Electronic Systems*, vol. 54, no. 1, pp. 90–105, Feb. 2018.

[10] J. A. Kovarskiy, R. M. Narayanan, A. F. Martone, K. D. Sherbondy, "A stochastic model for prediction and avoidance of RF interference to cognitive radars," *IEEE Radar Conf.*, Boston, MA, Apr. 2019.

[11] J. A. Kovarskiy, M. Kozy, C. Thornton, A. F. Martone, R. M. Narayanan, R. M. Buehrer, K. D. Sherbondy, "Comparing stochastic and Markov decision process approaches for predicting radio frequency interference," *Proc. SPIE, Radar Sensor Technology XXIII, 1100318*, Baltimore, MD, May 2019.

[12] B. Ravenscroft, J. W. Owen, J. Jakabosky, S. D. Blunt, A. F. Martone, K. D. Sherbondy, "Experimental demonstration and analysis of cognitive spectrum sensing and notching for radar," *IET Radar, Sonar, & Navigation*, vol. 12, no. 12, pp. 1466–1475, Dec. 2018.

[13] J. Owen, C. Mohr, B. Kirk, S. Blunt, A. Martone, K. Sherbondy, "Demonstration of real-time cognitive radar using spectrally-notched random FM waveforms," *IEEE Intl. Radar Conf.*, Washington, DC, Apr. 2020.

[14] J. Jakabosky, B. Ravenscroft, S. D. Blunt, A. Martone, "Gapped spectrum shaping for tandem-hopped radar/communications cognitive sensing," *IEEE Radar Conf,*, Philadelphia, PA, May 2016.

[15] C. Mohr, J. Owen, S. Blunt, "Zero-order reconstruction optimization of waveforms for modest DAC-rate systems," *IEEE Intl Radar Conf.*, Washington, DC, Apr. 2020.

[16] C. A. Mohr S. D. Blunt, "Analytical spectrum representation for physical waveform optimization requiring extreme fidelity," *IEEE Radar Conf.*, Boston, MA, Apr. 2019.

[17] H. Urkowitz, "Energy detection of unknown deterministic signals," *Proc. IEEE*, vol. 55, no. 4, pp. 523–531, Apr. 1967.

[18] A. F. Martone, K. D. Sherbondy, J. A. Kovarskiy, B. H. Kirk, C. E. Thornton, R. M. Buehrer, R. M. Narayanan, "Metacognition for radar coexistence," *IEEE Intl. Radar Conf.*, Washington, DC, Apr. 2020.